Genetic Algorithm Approach to Image Reconstruction in Electrical Impedance Tomography

Ho-Chan Kim*, Chang-Jin Boo*, Yoon-Joon Lee and Chang-Ik Kang*****

Abstract - In electrical impedance tomography (EIT), the internal resistivity distribution of the unknown object is computed using the boundary voltage data induced by different current patterns using various reconstruction algorithms. This paper presents a new image reconstruction algorithm based on the genetic algorithm (GA) via a two-step approach for the solution of the EIT inverse problem, in particular for the reconstruction of "static" images. The computer simulation for the 32 channels synthetic data shows that the spatial resolution of reconstructed images in the proposed scheme is improved compared to that of the modified Newton–Raphson algorithm at the expense of an increased computational burden.

Keywords: Electrical impedance tomography, Genetic algorithms, Image reconstruction, Inverse problem, Newton-Raphson method

1. Introduction

Electrical impedance tomography (EIT) plays an important role in monitoring tools for the process engineering such as biomedical, geological and chemical engineering, due to its relatively cheap electronic hardware requirements and non-intrusive measurement properties [1-3]. In EIT, different current patterns are injected to the unknown object through electrodes and the corresponding voltages are measured on its boundary surface. The physical relationship between inner resistivity (or conductivity) and boundary surface voltage is governed by the nonlinear Laplace equation with appropriate boundary conditions so that it is impossible to obtain the closed-form solution for the resistivity distribution. Hence, the internal resistivity distribution of the unknown object is computed using the boundary voltage data based on various reconstruction algorithms.

Yorkey et al. [4] developed a modified Newton-Raphson (mNR) algorithm for a static EIT image reconstruction and compared it with other existing algorithms such as backprojection, perturbation and double constraints methods. They concluded that the mNR reveals relatively good performance in terms of convergence rate and residual error compared to that of the other methods. However, in real situations, the mNR method often fails to obtain satisfactory images from physical data due to large modeling errors, poor signal to noise ratios (SNRs) and ill-conditioned (ill-posed) characteristics. That is, the ratio between the maximum and minimum eigenvalues of the information matrix (or Hessian matrix) is very large. In particular, the ill-conditioning of the information matrix results in an inaccurate matrix inverse so that the resistivity update process is very sensitive to the modeling and measurement errors.

Genetic algorithms (GAs) have recently found extensive applications in solving global optimization searching problems [5]. They are useful when the closed-form optimization technique cannot be applied. GAs are parallel, global search techniques that emulate natural genetic operators. Because a GA simultaneously evaluates many points within a parameter space, it is more likely to converge toward the global solution. It does not need to assume that the search space is differentiable or continuous, and can also iterate several times on each datum received. The GAs apply operators inspired by the mechanics of natural selection to a population of binary strings encoding the parameter space. At each generation, it explores different areas of the parameter space, and then directs the search to regions where there is a high probability of finding improved performance. By working with a population of solutions, the algorithms can in effect search for many local minima, and thereby increase the likelihood of finding the global minimum. Global optimization can be achieved via a number of genetic operators, e.g., reproduction, mutation, and crossover.

In the EIT for two-phase flow visualization, the cross-sectional resistivity distribution of each phase at a certain instance is reconstructed as an image. The major difficulties

* Dept. of Electrical Engineering, Cheju National University, Korea. (hckim@cheju.ac.kr)
** Dept. of Nuclear and Energy Engineering, Cheju National University, Korea. (leeyj@cheju.ac.kr)
*** Dept. of Marine Instrumentation Engineering, Cheju National University, Korea. (cikang@cheju.ac.kr)
Received January 5, 2004 ; Accepted April 28, 2004

in impedance imaging are in the nonlinearity of the problem itself and the poor sensitivity of the boundary voltages to the resistivity of the flow domain deep inside. Several researchers suggested various element or mesh grouping methods where they force all meshes belonging to certain groups to have identical resistivity values [6, 7].

In this paper, we will discuss the image reconstruction in EIT based on GA via a two-step approach. We have broken the procedure for obtaining the internal resistivity distribution into two parts. In the first step, each mesh is classified into three mesh groups: target, background, and temporary groups. The mNR algorithm can be used to determine the group region. In the second step, the values of these resistivities are determined using the genetic algorithm. This two-step approach allows us to better constrain the inverse problem and subsequently achieve a higher spatial resolution.

2. Image reconstruction using GA in EIT

The numerical algorithm used to convert the electrical measurements at the boundary to a resistivity distribution is described here. The algorithm consists of iteratively solving the forward problem and updating the resistivity distribution as dictated by the formulation of the inverse problem. The forward problem of EIT calculates the boundary measurements given the electrical resistivity distribution, and the inverse problem of EIT takes potential measurements at the boundary and forms an image of the resistivity distribution.

2.1 The forward problem

When electrical current $I_l(l=1,\cdots,L)$ is injected into the object $\Omega \in R^2$ through the electrode $e_l(l=1,\cdots,L)$ attached on the boundary $\partial\Omega$, and the resistivity distribution $\rho(x,y)$ is known for the Ω, the corresponding induced electrical potential $u(x,y)$ can be determined uniquely from the nonlinear Laplace equation, which in turn can be derived from the Maxwell equation, Ohm's law, and the Neumann type boundary condition. The complete electrode model takes into account both the shunting effect of the electrode and the contact impedances between the electrodes and tissue. The equations of the complete electrode model are

$$\nabla \cdot (\rho^{-1} \nabla u) = 0 \text{ in } \Omega \tag{1}$$

$$\begin{aligned} &\int_{e_l} \rho^{-1} \frac{\partial u}{\partial n} dS = I_l,\ l=1,\cdots,L \\ &u + z_l \rho^{-1} \frac{\partial u}{\partial n} = U_l \text{ on } e_l,\ l=1,\cdots,L \\ &\rho^{-1} \frac{\partial u}{\partial n} = 0 \text{ on } \partial\Omega \setminus \bigcup_{l=1}^{L} e_l \end{aligned} \tag{2}$$

where z_l is effective contact impedance between l th electrode and tissue, U_l is the measured potentials and n is outward unit normal. In addition, we have the following two conditions for the injected currents and measured voltages by taking into account the conservation of electrical charge and appropriate selection of ground electrode, respectively.

$$\sum_{l=1}^{L} I_l = 0 \tag{3}$$

$$\sum_{l=1}^{L} U_l = 0 \tag{4}$$

The computation of the potential $u(x,y)$ for the given resistivity distribution $\rho(x,y)$ and boundary condition I_l is called the forward problem. The numerical solution for the forward problem can be obtained using the finite element method (FEM). In the FEM, the object area is discretized into small elements having a node at each corner. It is assumed that the resistivity distribution is constant within an element. The potential at each node is calculated by discretizing (1) into $Y\upsilon = c$, where $Y \in R^{N \times N}$ is so-called stiffness matrix and N is the numbers of FEM nodes. Y and c are the functions of the resistivity distribution and the injected current patterns, respectively.

2.2 The inverse problem

The inverse problem, also known as the image reconstruction, consists in reconstructing the resistivity distribution $\rho(x,y)$ from potential differences measured on the boundary of the object. Ideally, knowing the potential of the entire boundary makes the correspondence between the resistivity distribution and the potential biunivocal. The relatively simple situation depicted so far does not hold exactly in the real world. The methods used for solving the EIT problem search for an approximate solution, i.e., for a resistivity distribution minimizing some sort of residual involving the measured and calculated potential values. From a mathematical point of view, the EIT inverse problem consists in finding the coordinates of

a point in a N-dimensional hyperspace, where N is the number of discrete elements whose union constitutes the tomographic section under consideration. In the past, several EIT image reconstruction algorithms for the current injection method have been developed by various authors. A review of these methods is given in [8]. To reconstruct the resistivity distribution inside the object, we must solve the nonlinear ill-posed inverse problem. Regularization techniques are needed to obtain stable solutions due to the ill-posedness.

A generalized Tikhonov regularized version of the EIT inverse problem can be written in the form

$$\Psi(\rho) = \min_{\rho}\{\| V - U(\rho) \|^2 + \alpha \| R(\rho - \rho^*) \|^2\} \tag{5}$$

where $\rho \in R^N$ and ρ^* are the resistivity distribution and a priori information of ρ, respectively. $U(\rho) \in R^{LK}$ is the vector of voltages obtained from the model with known ρ, $V \in R^{LK}$ are the measured voltages and R and α are the regularization matrix and the regularization parameter, respectively. L, K, and M are the numbers of electrodes on the surface, injected current patterns, and finite elements in FEM respectively. There are many approaches in the literature [9-12] to determine R and α, but the usual choice is to fix $R = I_N$ and to adjust α empirically.

Minimizing the objective function $\Psi(\rho)$ gives an equation for the update of the resistivity vector

$$\begin{aligned} \rho^{k+1} &= \rho^k + \Delta\rho^{k+1} \\ \Delta\rho^k &= (H_k + \alpha I)^{-1}\{J_k^T (V - U(\rho^k)) - \alpha(\rho^k - \rho^*)\} \end{aligned} \tag{6}$$

where the partial derivative of Ψ with respect to ρ has been approximated by a Taylor series expansion around ρ^k. The Jacobian J_k is a matrix composed of the derivative of the vector of predicted potentials with respect to the unknown resistivities. The Jacobian is derived from the finite element formulation given by $J_k = \left.\frac{\partial \Psi}{\partial \rho}\right|_{\rho^k}$. The Hessian H_k is the second derivative of the predicted potentials with respect to the resistivity and is approximated as the square of the Jacobian for computational efficiency. Since the objective function $\Psi(\rho)$ is multimodal (i.e., it presents several local minima), the inversion procedure does not always converge to the true solution. The reconstruction algorithms are likely to be trapped in a local minimum and sometimes the best solution of a static EIT problem is rather unsatisfactory.

In particular, two characteristics of genetic algorithms appear to be of value in EIT reconstruction; no evaluation of function derivatives is needed and no assumption on function continuity needs to be made. The preceding considerations suggest the viability of employing GA's for the solution of the EIT problem, according to the procedure described in the following section.

2.3 The GA approach to EIT

In two-phase flow fields, we may assume that there are only two different representative resistivity values; one resistivity value for the background and the other for the target. Here, the target need not be a single segment. It may be multiple segments of the same resistivity value.

In this paper, we will discuss the image reconstruction in EIT using a two-step approach. We have broken the procedure for obtaining the internal resisitivity distribution into two parts. In the first step, we adopted a mNR method as a basic image reconstruction algorithm. After a few initial mNR iterations performed without any grouping, we classify each mesh into one of three mesh groups: BackGroup (or TargetGroup) is the mesh group with the resistivity value of the background (or target). TempGroup is the group of meshes neither in BackGroup nor in TargetGroup. All meshes in BackGroup and in TargetGroup are forced to have the same but unknown resistivity value (ρ_{back} and ρ_{tar}), respectively. However, all meshes in TempGroup can have different resistivity values ($\rho_{temp,i}$, $i = 1, \cdots, n-2$).

In the simplest implementation of GA in EIT, a set (population) of EIT images is generated, usually at random. Each individual consists in a n-tuple of resistivity values (n is the number of elements discretizing the section under measurement), i.e., the EIT chromosome is a sequence of n resistivities. After mesh grouping, in this paper, we will determine the values of these resistivities using two GAs. The first GA searches for the optimal range of resistivities by generating and evolving a population of individuals whose chromosome consists of two real genes (ρ_{back} and ρ_{tar}), representing the BackGroup and TargetGroup values of the unknown resistivity distribution. Furthermore, we will use ρ_{back} (or ρ_{tar}) as the minimum (or maximum) values of the unknown resistivity distribution. The population randomly generated in this first GA is constrained between the minimum and maximum resistivities obtained in the first GA. The second GA solves the EIT problem, searching for the resistivity distribution ($\rho_{temp,i}$, $i = 1, \cdots, n-2$) minimizing the reconstruction error. The computed resistivities are constrained between the minimum and maximum values

obtained in the first GA.

A fitness value is computed for each individual. In the present case, the fitness function is the reciprocal of the reconstruction error, a function of the relative difference between the computed and measured potentials on the object boundary

$$f_c = \frac{L(L-1)}{2}\left[\sum_{i=1}^{L(L-1)/2}\left|\frac{V_i(\rho)-U_i}{U_i}\right|\right]^{-1} \tag{7}$$

where L is the number of electrodes on the surface.

The next step is to rank the individuals on their fitness value, giving the fitter ones more chance to contribute to the successive generation. New individuals are then created by crossover (combination of couples of resistivity sequences) and mutation (low-probability random change of some resistivity value in the genome).

After this step, the chosen termination criterion is applied, i.e., we see if convergence has been reached (the residue is below a given value) or if the maximum number of generations has been exceeded. If convergence fails, the whole selection+crossover+mutation procedure is applied to the current population, otherwise the fittest individual is assumed as the solution of the EIT problem. The termination condition adopted here is based on evaluating the progress made by the algorithm in a predefined number of generations and terminating the search if the fitness of the best chromosome is above the threshold value.

3. Computer simulation

The proposed algorithm has been tested by comparing its results for numerical simulations with those obtained by the modified Newton–Raphson (mNR) method. In order to test the proposed algorithm, the complete electrode model with the finite element method (FEM) was used to calculate the measurements V. For the current injection the trigonometric current patterns were used. For the forward calculations, the domain Ω is the unit disc and the mesh of 3104 triangular elements (M=3104) with 1681 nodes (N=1681) and 32 channels (L=32) was used as shown in Fig. 1(a). The FEM elements were grouped together such that a total of 776 elements (M=776) with 453 nodes (N=453) were obtained for the inverse calculations as shown in Fig. 1(b). In this paper, under the assumption that the resistivity varies only in the radial direction within a cylindrical coordinate system, the results of the two inverse problem methods can be easily compared. The resistivity profile given to the finite element inverse solver varies from the center to the boundary of the object and is divided into 9 radial elements ($\rho_1, \cdots, \rho_9$) in Fig. 1(a).

The resolution of the method is determined by a number of variables including resistivity contrast and distribution, position within the vessel, and even current pattern. The ability to positively distinguish between two similar resistivity distributions also depends upon the precision of the voltage measurements. These factors necessitate caution when designing an experiment and interpreting results. Therefore, to verify the appropriateness of EIT for this application, a computational experiment was conducted.

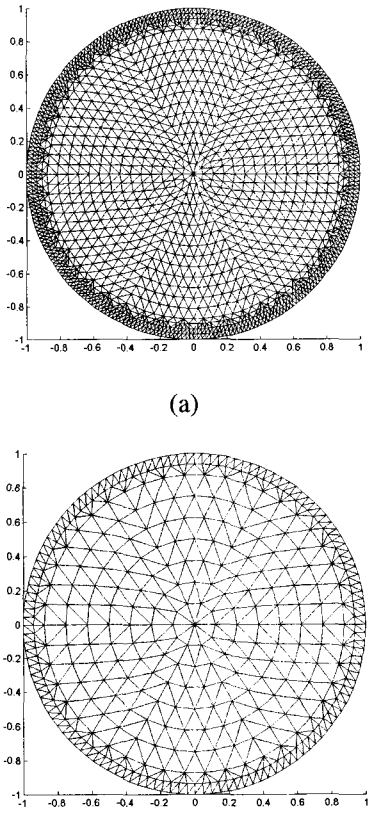

(a)

(b)

Fig. 1 The Finite element mesh used in the calculation. (The resistivities of the elements within an annular ring are identi cal.) (a) mesh for forward solver, (b) mesh for inverse solver.

Synthetic boundary potentials were computed for idealized resistivity distributions using the finite element method described earlier. The boundary potentials were then used for inversion and the results were compared to the original resistivity profiles. The resistivity profile appearing in Fig. 2 contains two large discontinuities in the original resistivity distribution. The evaluation of the algorithm using large step changes at r/R =0.56 and 0.81 is a severe test on the inverse method, which it handles well, since smoother variations in resistivity are expected.

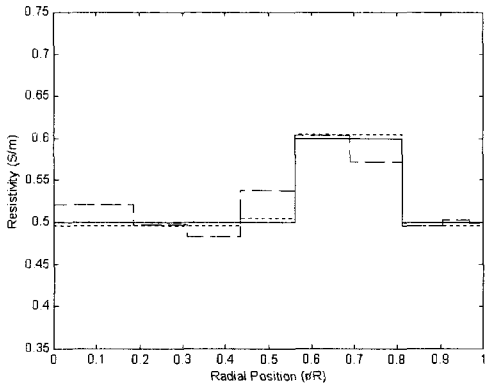

Fig. 2 True resistivities (solid line) and computed resistivities using mNR (dashed line) and GA (dotted line).

We started the mNR iteration without any mesh grouping with a homogeneous initial guess. In Table 1, we see that the mNR algorithm may roughly estimate the given true resistivities. Since the mNRs have a large error at the boundary of target and background in Fig. 2, we cannot obtain reconstructed images of high spatial resolution. This kind of poor convergence is a very typical problem in the NR-type algorithms.

However, we can significantly improve the mNR's poor convergence by adopting the proposed GA via a two-step approach as follows.

Table 1 True resistivities and computed resistivities using mNR and GA

	ρ_1	ρ_2	ρ_3	ρ_4	ρ_5	ρ_6	ρ_7	ρ_8	ρ_9
Real	0.5	0.5	0.5	0.6	0.6	0.6	0.6	0.6	0.6
mNR	.516	.495	.489	.535	.594	.604	.599	.601	.600
GA	.505	.505	.505	.600	.600	.600	.600	.600	.600

In the first step, we adopted a mNR method as a basic image reconstruction algorithm. After a few initial mNR iterations performed without any grouping, we classified each mesh into one of three mesh groups. As shown in Table 1, it should be noted that 2 meshes (ρ_5, ρ_6) and 5 meshes $(\rho_2, \rho_3, \rho_7, \rho_8, \rho_9)$ among 9 are grouped into TargetGroup (ρ_{tar}) and BackGroup (ρ_{back}), respectively. The remaining meshes (ρ_1, ρ_4) are grouped into TempGroup. Hence, the number of unknowns is reduced to 4.

In the second step, after mesh grouping, we will determine the values of these resistivities using two GAs. The first GA searches for the optimal range of resistivities by generating and evolving a population of individuals whose chromosome consists of two real genes (ρ_{back} and ρ_{tar}), representing the BackGroup and TargetGroup values of the unknown resistivity distribution. Furthermore, we will use ρ_{back} (or ρ_{tar}) as the minimum (or maximum) values of the unknown resistivity distribution. The initial value of ρ_{tar} and ρ_{back} are the average resistivity values of meshes in BackGroup and TargetGroup, respectively. Table 2 shows the computed resistivities as a function of the population size at generation 200. The reconstructed errors at a given generation generally decrease when the population size is increased. Hence, even if error does not depend linearly on the population size due to the stochastic nature of GA's, 40 or 60-individual GA reconstructions gives a higher spatial resolution than a mNR method.

Table 2 True and computed resistivities using GA vs. population size at generation 200

Pop. size	ρ_{back}		ρ_{tar}	
	True	Computed	True	Computed
20	0.5	0.5031	0.6	0.5685
40	0.5	0.4954	0.6	0.6038
60	0.5	0.4998	0.6	0.6039

The second GA solves the EIT problem, searching for the resistivities of remainders (ρ_1, ρ_4) minimizing the reconstruction error. The computed resistivities in this second GA are constrained between the minimum and maximum values obtained in the first GA. In Fig. 1, the inverted profile using GA matches the original profile very well near the wall at r/R=1.0 as well as the center at r/R =0.0. Furthermore, the GA reconstruction is practically perfect for the jump of resistivty at r/R =0.56 and 0.81.

4. Conclusion

In this paper, an EIT image reconstruction method based on GA via a two-step approach was present to improve the spatial resolution. A technique based on two binary-coded GAs with the knowledge of mNR was developed for the solution of the EIT inverse problem. One GA calculates the resistivity values of the target group and background group, and the other GA is used to search for the resistivities of remainders. Although GA is expensive in terms of computing time and resources, which is a weakness of the method that renders it presently unsuitable for real-time tomographic applications, the exploitation of a priori knowledge produces very good reconstructions. Further extensions include an EIT image reconstruction to multi-phase flow fields.

Acknowledgements

This work was supported by the Nuclear Academic Research Program of the Ministry of Science and Technology (MOST).

References

[1] J. G. Webster, Electrical Impedance Tomography, Adam Hilger, 1990.

[2] J. C. Newell, D. G. Gisser, and D. Isaacson, "An electric current tomograph," *IEEE Trans. on Biomedical Engineering*, vol. 35, no. 10, pp. 828-833, 1987.

[3] M. Cheney, D. Isaacson, and J. C. Newell, "Electrical impedance tomography," *SIAM Review*, vol. 41, no. 1, pp. 85-101, 1999.

[4] T. J. Yorkey, J. G. Webster, and W. J. Tompkins, "Comparing reconstruction algorithms for electrical impedance tomography," *IEEE Trans. on Biomedical Engineering*, vol. 34, no. 11, pp. 843-852, 1987.

[5] D. E. Goldberg, Genetic Algorithms in Search, Optimization and Machine Learning. Reading, MA: Addison Wesley, 1989.

[6] M. Glidewell and K. T. Ng, "Anatomically constrained electrical impedance tomography for anisotropic bodies via a two-step approach," *IEEE Trans. on Medical Imaging*, vol. 14, no. 3, pp. 498-503, 1995.

[7] K. D. Paulsen, P. M. Meaney, M. J. Moskowitz, and J.M. Sullivan, "A dual mesh scheme for finite element based reconstruction algorithm," *IEEE Trans. on Medical Imaging*, vol. 14, no. 3, pp. 504–514, 1995.

[8] T. Murai and Y. Kagawa, "Electrical impedance computed tomography based on a finite element model," *IEEE Trans. on Biomedical Engineering*, vol. 32, no. 3, pp.177-184, 1985.

[9] C. Cohen-Bacrie, Y. Goussard, and R. Guardo, "Regularized reconstruction in electrical impedance tomography using a variance uniformization constraint," *IEEE Trans. on Medical Imaging*, vol. 16, no. 5, pp. 170-179, 1997.

[10] M. Vauhkonen, D. Vadasz, P. A. Karjalainen, and J. P. Kaipio, "Subspace regularization method for electrical impedance tomography," *1st International Conference on Bioelectromagnetism*, Tampere, Finland, pp. 9-13, 1996.

[11] A. Adler and R. Guardo, "Electrical impedance tomography: regularized imaging and contrast detection," *IEEE Trans. on Medical Imaging*, vol. 15, no. 2, pp. 170-179, 1996.

[12] C. J. Grootveld, A. Segal, and B. Scarlett, "Regularized modified Newton-Raphson technique applied to electrical impedance tomography," John Wiley & Sons, *International Journal of Imaging System Technology*, vol. 9, pp. 60-65, 1998.

Ho-Chan Kim

He received his B.S., M.S., and Ph.D. degrees in Control & Instrumentation Engineering from Seoul National University in 1987, 1989, and 1994, respectively. He was a Research Staff Member between 1994 and 1995 at the Korea Institute of Science and Technology (KIST). Since 1995, he has been with the Department of Electrical Engineering at Cheju National University, where he is currently an Associate Professor. He was a Visiting Scholar at Pennsylvania State University from 1999 to 2000. His research interests include robust adaptive control, wind control, and power control.

Chang-Jin Boo

He received his B.S. and M.S. degrees in Electrical Engineering from Cheju National University in 2001 and 2003, respectively. He is currently a Ph.D. student at Cheju National University. His research interests include embedded and RT system control.

Yoon-Joon Lee

He received his B.S. (Seoul National Univ., 1975), M.S. (Penn State Univ., 1980), and Ph.D. degree (Seoul National Univ., 1990) in Nuclear Engineering. He worked as a Nuclear Engineer from 1975 to 1978, and has 8 years of experience in plant design. He has worked in the Department of Nuclear and Energy Engineering of Cheju National University since 1984. His major interest is the automatization of nuclear plant operations.

Chang-Ik Kang

He received his B.S., M.S., and Ph.D. degrees in Control & Instrumentation Engineering from Seoul National University in 1989, 1991, and 1995, respectively. From 1995 to 1999, he was an Engineer in the Storage Division of Samsung Electronics. Since 1999, he has been with the Department of Marine Instrumentation Engineering at Cheju National University, where he is currently an Assistant Professor. His research interests include control of data storage systems, nonlinear control, and sonar signal processing.